International Journal for Housing Science and Its Applications
Publish August 4, 2025. Volume 46, Issue 3 Pages 2812-2824

https://doi.org/10.70517/ijhsa463236

Design and Implementation of a Fuzzy Decision-Making Method for a Robot Vision System for Unloading Operations

Fei Yuan[1,*]
[1] Wuxi Vocational and Technical College of Commerce, Wuxi, Jiangsu, 214153, China
Corresponding authors: (e-mail: yuanfei@wxic.edu.cn).

Abstract In order to solve the problems of high labor intensity, high safety risk and low efficiency of manual loading and unloading under high temperature and high noise environments, this paper designs a loading and unloading control system based on the 3D high-precision vision guidance technology with PLC equipment as the control platform and a six-axis industrial robot as the flexible drive source, and constructs the position servo mathematical model of the unloading equipment under the perturbed working condition, and utilizes the fuzzy neural network PID (FNN-) PID) control algorithm to realize the position control optimization of the loading and unloading equipment. the output parameters K_p, T_i and T_d of the FNN-PID control algorithm can adaptively change the output values based on the fuzzy rule-base with the change of inputs, and it can inhibit the swing angle of the lanyard from 12 degrees to be stabilized at 0 degrees within 24s. Nearby, the tracking effect and anti-swing effect are significantly better than FPID control. This paper adopts the robot vision guidance unloading, so that the unloading control system has obvious improvement in the guiding speed and accuracy, and has high engineering application value.

Index Terms robot, 3D visual guidance, fuzzy neural network PID control, unloading control

I. Introduction

Industrial robots have good maneuverability and flexibility and are an important part of industrial manufacturing systems [1]. Robots function as the equivalent of human hands in industrial manufacturing systems, realizing the handling, sorting, and loading and unloading of target workpieces, and are increasingly used in various fields of industrial production [2]. However, most of the industrial robots work in a pre-determined environment, in which they are schematically taught through a pre-programmed program and then run according to a fixed trajectory [3], [4]. Generally the actual position of the target workpiece and the ideal situation usually also exist a certain error, the existence of these errors may lead to the robot can not work as expected, resulting in robot work errors [5]-[7]. With the progress of science and technology, in order to solve the shortcomings of traditional robots in industrial production, the introduction of robotic products with machine vision function.

Machine vision technology is through industrial robots or industrial cameras to help industrial robots to realize the automation of parts grasping, loading and unloading, processing, handling and other functions, to achieve the purpose of improving production efficiency and reducing production costs [8]. Compared with the limitations of manual labor, the use of industrial robots with vision assistance can complete more intense, dangerous, high precision and high task operations [9], [10]. Accompanied by intelligent manufacturing to the entire manufacturing industry to bring a huge impact, while facing more flexible production tasks or more types of parts processing, so the need for industrial robotics field also requires a higher degree of flexibility, precision, accuracy to meet the more heavy workload [11]-[14]. For robotic workpiece localization systems for loading and unloading tasks, it is necessary to propose visual guidance optimization strategies with better recognition effects to meet the increasingly heavy industrial production tasks [15], [16].

In this paper, the robot is combined with 3D visual guidance technology to realize the unloading control system building, and construct the unloading equipment dynamics model and visual projection model under the disturbed working condition, at the same time, the traditional fuzzy PID is improved, and combined with the fuzzy control and the neural network, the optimization algorithm for the unloading equipment position control based on the fuzzy neural network PID is proposed. In order to test the effectiveness of the FNN-PID control algorithm, it is compared with the fuzzy PID control algorithm for tracking and anti-shaking effect. Finally, the practical efficacy of the control system is evaluated from three aspects: guidance accuracy, visual processing quality and unloading control effect.

II. Unloading control system based on vision guidance and robot drive

In this chapter, the unloading control system based on vision guidance and industrial robot drive is designed by taking the long water spout of continuous casting ladle as an example, and the equipment of the system contains one set of industrial robot, robot quick-change device, PLC control system, HMI human-machine interaction system, long water spout and long water spout unloading tooling, industrial camera, and vision computing platform. Among them, PLC control cabinet, robot control cabinet, HMI monitoring screen, long spout device and long spout unloading tooling workstations are arranged nearby in the safe area of the site. The top view of the equipment layout is shown in Figure 1.

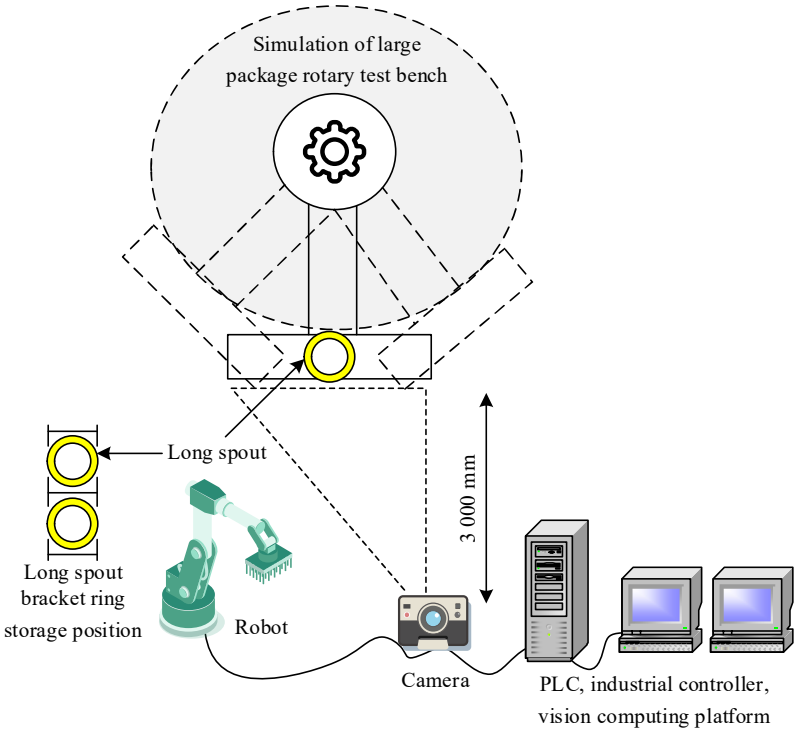

Figure 1: Top view of the system equipment layout

The control system mainly consists of network communication subsystem, PLC logic control system, human-machine interaction system, industrial robot drive system and 3D vision guidance system. The long spout and storage rack equipment contains long spout, emergency long spout, spout unloading tooling, and long spout holder. The design of the long spout bracket makes gripping the long spout simple and easy, its bayonet and bracket ring are connected through the guide post, the spring ensures the pre-pressure, the bracket ring holds the long spout, the bayonet hangs on the post hook of the ladle sliding spout, and the long spout bracket ring is equipped with the visual feature recognition board and the robotic gripping operation hole. The long spout unloading workpiece is selected to carry the long spout, the front end of the two pins and the long spout bracket ring, the tail end of the robot connected to the quick-change tool female head. The long spout bracket and other equipment is fixed on the pouring steel platform, the bracket fixes the position and direction of the long spout, and it is also equipped with sensors, which are not movable and should be placed according to the requirements, so as to facilitate the robot's gripping and PLC logic control.

III. Robot vision-guided unloading control models

III. A. Mathematical modeling of the position of unloading equipment under disturbed working conditions

In this section, the mathematical model of positional attitude under disturbed working conditions is constructed by taking the crane for lifting as an example, which lays the foundation for robot vision-guided positional control optimization of unloading equipment.

III. A. 1) Lifting dynamics model

The simplified model of four-degree-of-freedom lifting is shown in Fig. 2, with G denoting the world coordinate system, v_x denoting the motion velocity of the large vehicle traveling device along the X-axis, v_y denoting the

motion velocity of the small vehicle traveling device along the Y-axis, v_z denoting the motion velocity of the heavy object along the Z-axis, and ω_φ denoting the rotational angular velocity of the heavy object around the Z-axis.

Ideally, the lifting dynamics model can be expressed as:

$$M(\eta)\dot{v} + C(\eta, v)v + G(\eta) = Q \tag{1}$$

where $\eta = [x, y, z, \varphi, 0, 0]^T \in \mathbb{R}^6$ denotes the positional state vectors of the weight, including the displacement vector $\eta_a = [x, y, z]^T$ and angle vectors $\eta_b = [\varphi, 0, 0]^T$, $v = [v_x, v_y, v_z, \omega_\varphi, 0, 0]^T \in \mathbb{R}^6$ denotes the velocity vector of motion, including the linear velocity vector $v_a = [v_x, v_y, v_z]^T$ and the angular velocity vector $v_b = [\omega_\varphi, 0, 0]^T$. $M(\cdot) > 0$ denotes the positive definite inertia matrix of the system, $C(\cdot)$ is the Coriolis centripetal matrix, $G(\cdot)$ denotes the gravity vector, and Q denotes the control vector.

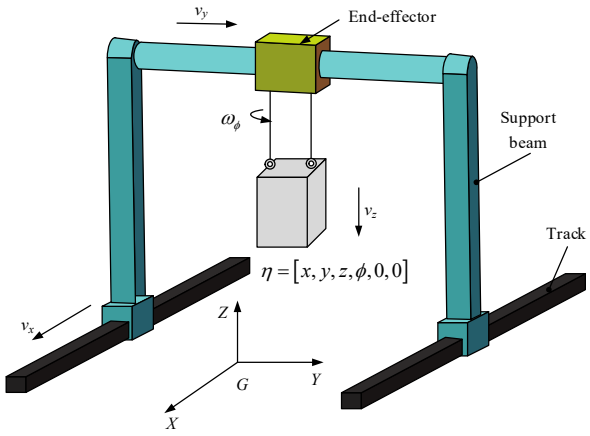

Figure 2: Model of hoisting crane

However, in the actual lifting and positioning project, taking into account the uncertainty and external interference due to the lifting equipment's own factors, this paper introduces the perturbation term, and describes the lifting dynamics equations as follows:

$$M(\eta)\dot{v} + C(\eta, v)v + G(\eta) + D(v) = Q + \tau \tag{2}$$

where $D(v)$ denotes the damping term and τ denotes the perturbation term.

III. A. 2) **Visual projection models**

The camera is fixed to the lifting end-effector in the form of a “hand-on-eye”, and the visual projection model is shown in Figure 3. Assuming that the camera coordinate system C coincides with the center of the end-effector, the camera and the end-effector have the same position and motion speed. G denotes the world coordinate system and C^* denotes the desired position camera coordinate system.

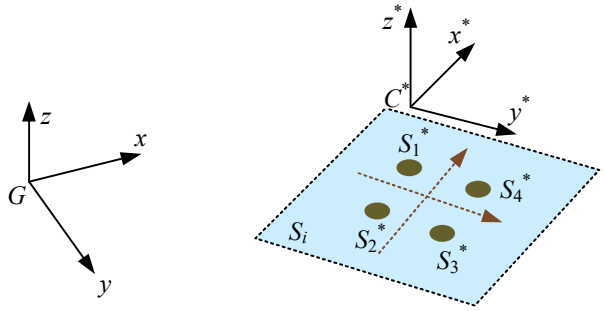

Figure 3: Visual projection

$S_i = (X_i, Y_i, Z_i)^T$ and $S_i^* = (X_i^*, Y_i^*, Z_i^*)^T$ denote respectively the camera coordinate system C and the coordinates of feature points in the desired position camera coordinate system C^*, which can be obtained by differentiating S_i:

$$\dot{S}_i = v_a + v_b \times S_i \tag{3}$$

According to the relationship between focal length and imaging, it can be obtained:

$$\begin{cases} x_i = \dfrac{l}{Z_i} X_i \\ y_i = \dfrac{l}{Z_i} Y_i \end{cases} \tag{4}$$

where: l denotes the focal length, and x and y denote the image physical coordinates.

Then, image coordinate system to pixel coordinate system conversion is performed:

$$\begin{cases} u = \dfrac{x_i}{dx} + u_0 = \alpha_1 x_i + u_0 \\ v = \dfrac{y_i}{dy} + v_0 = \alpha_2 y_i + v_0 \end{cases} \tag{5}$$

where: α_1 denotes the number of pixels per unit distance in the x direction, while α_2 denotes the number of pixels in the y direction, and u_0, v_0 denote the origin of the image plane.

According to the principle of perspective projection, the coordinates of the feature points in the image coordinate system and the desired coordinate system are calculated:

$$s_i = [u_i, v_i]^T = \frac{F}{Z_i}[x_i, y_i]^T \tag{6}$$

$$s_i^* = [u_i^*, v_i^*]^T = \frac{F}{Z_i}[x_i^*, y_i^*]^T \tag{7}$$

where: $F = \begin{bmatrix} \alpha_1 l & 0 \\ 0 & \alpha_2 l \end{bmatrix}$, and u_i, v_i denote the coordinates of the feature point in the pixel coordinate system.

According to the target feature differential equation, the relationship between image features, visual Jacobi matrix and motion velocity can be defined in this way:

$$\dot{s}_i = J_c v \tag{8}$$

where: v denotes the motion velocity, and J_c is a Jacobi matrix dependent on the camera parameters and image depth.

According to the real-time target feature s and the desired target feature s^*, then the image feature error can be expressed as follows:

$$e = s - s^* \tag{9}$$

Differentiating the above equation in the case where s^* is a constant yields

$$\dot{e} = J_c v \tag{10}$$

III. B. ***Optimization of position control based on fuzzy neural network PID***

In this section, for the defects of the traditional PID [17], fuzzy control and neural network are introduced to improve the PID control, and the fuzzy PID as well as fuzzy neural network PID controllers are designed with the mathematical model of the position control system of the unloading equipment to achieve the optimization of the position control of the equipment.

III. B. 1) **Fuzzy Neural Networks**

The two intelligent optimization algorithms, fuzzy control and neural network, are complementary and can be combined to form a fuzzy neural network (FNN) [18], which possesses both the inference function of fuzzy control and the self-regulation and self-learning function of neural network.

The fuzzy neural network structure is shown in Fig. 4. The first layer is the input layer, which is directly connected to the inputs and acts as a bridge between the inputs and the second layer, which can directly transfer the inputs to the second layer. The input and output of this layer is represented as:

$$f_1(i) = x_i \tag{11}$$

where x_i is the node input $i = 1, 2, \cdots, m$, representing the number of fuzzy inputs, and $f_1(i)$ represents the output of the network.

The second layer is the affiliation function layer, each node in this layer represents a fuzzy subset and the function is to find the affiliation of the input values. The affiliation function is a Gaussian type function, c_{ij} and b_{ij} denote the center value and width of the affiliation function of the j fuzzy set for the i input value, respectively, and $j = 1, 2, \cdots, n_i$ denotes the number of linguistic variables for each input variable. The number of nodes in the layer is $N_2 = \sum_{i=1} n_i$, and the output of the layer is represented as:

$$\mu_i^j = \exp\left(net_j^2\right) \tag{12}$$

$$net_j^2 = -\frac{(x_i - c_{ij})^2}{(b_{ij})^2} \tag{13}$$

The third layer is the rule layer, which is used to calculate the fitness of each rule, and any node in this layer corresponds to a fuzzy control rule in the rule base, i.e., there are a total of $N_3 = n = \prod_{i=1}^{m} n_i$ nodes in this layer. If $j = 1, 2, 3, \cdots, n$, $i_1 \in \{1, 2, \cdots, n_1\}$, $i_2 \in \{1, 2, \cdots, n_2\}$, $i_m \in \{1, 2, \cdots, n_m\}$, then:

$$\alpha_j = \mu_{i_1}^{i_1} \cdot \mu_{i_2}^{i_2} \cdot \cdots \cdot \mu_{i_m}^{i_m} \tag{14}$$

Or:

$$\alpha_j = \min\left\{\mu_{i_1}^{i_1}, \mu_{i_2}^{i_2}, \cdots, \mu_{i_m}^{i_m}\right\} \tag{15}$$

The fourth layer is the normalization layer, which has the same number of nodes as the previous layer, i.e., $N_4 = n$, and its output is:

$$\bar{\alpha}_j = \frac{\alpha_j}{\sum_{j=1}^{n} \alpha_j}, j = 1, 2, \cdots, n \tag{16}$$

The fifth layer is the output layer with f_5, i.e., the output:

$$y_k = W \cdot \bar{\alpha}_j = \sum_{j=1}^{n} \omega_{kj} \cdot \bar{\alpha}_j \tag{17}$$

where $k = 1, 2 \cdots r$ is the number of nodes in the output layer, and W is the link weight matrix of the output layer nodes to the nodes in the fourth layer.

III. B. 2) **Fuzzy neural network PID controller design**

For the shortcomings of fuzzy PID (FPID) control, this paper designs a position control algorithm for unloading equipment based on fuzzy neural network PID (FNN-PID) [19]. FNN-PID is a control algorithm that combines fuzzy control, neural network, and PID, and it can make the PID, which is widely used in industrial control, possess both the experience and rules of fuzzy control and the self-regulation and learning function of neural network. The structure of the fuzzy neural network PID control system is shown in Figure 5.

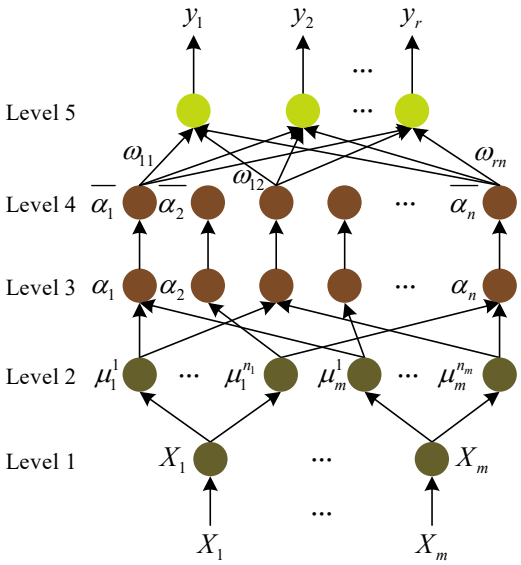

Figure 4: Fuzzy neural network structure

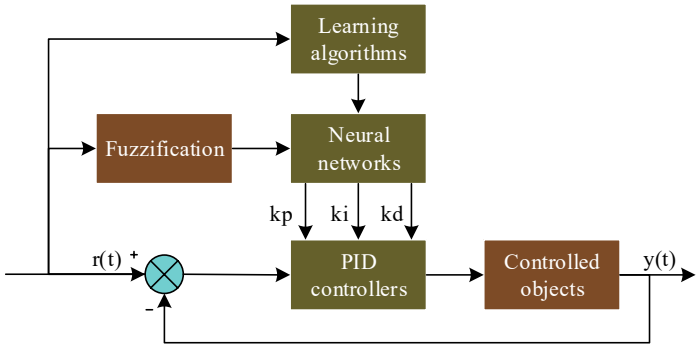

Figure 5: Structure of Fuzzy Neural Network PID Control System

Combining the characteristics of position control of unloading equipment and the functional structure of FNN-PID algorithm, this paper designs a two-input and three-output fuzzy neural network PID control system. The input is the difference e between the actual speed of the motor and the desired speed and the rate of change of the difference ec, and the output is the three parameters k_p, k_i and k_d of the PID control. The network structure and specific parameters are designed as follows:

(1) Determine the input variables of the input layer

In the stacker position control system, it mainly controls the rotational speed of the motor, so the inputs of the first layer of FNN_PID are the rotational speed difference e and the rate of change of the difference ec, and these two inputs are passed to the next layer, so the total number of nodes in this layer is $N_1 = 2$.

(2) Affiliation function layer design

Seven nodes are set for e and ec respectively, so there are a total of $N_2 = 14$ nodes in this layer, representing seven fuzzy linguistic variables, namely $\{NB, NM, NS, ZO, PS, PM, PB\}$. This layer is mainly to find the value of the affiliation function of the subset of 7 linguistic variables according to Eq. (12) and Eq. (13).

(3) Rule layer design

Each node in this layer represents a fuzzy control rule. Since there are 2 inputs in the input layer and each input has 7 linguistic fuzzy subsets in the affiliation function layer, it corresponds to 49 network nodes in this layer.

(4) Design of the normalization layer

The function of this layer is to implement the normalization process and call Eq. (16) for computation. The nodes in this layer are the same as in the previous layer, i.e., $N_4 = 49$.

(5) Design of output layer

This design has a total of three outputs for the three parameters of PID: k_p, k_i and k_d. So the number of nodes in this layer is $N_5 = 3$, where $y_1 = k_p$, $y_2 = k_i$ and $y_3 = k_d$. Multiply the weights of the neurons in this layer with the normalized result of the previous layer, and then take the sum respectively, the value obtained is the output value of this layer, which is calculated as shown in Eq. (17), and expressed in vector formula as follows:

$$y = \begin{bmatrix} y_1 \\ y_2 \\ y_3 \end{bmatrix} = \begin{bmatrix} \omega_{11} & \omega_{12} & \cdots & \omega_{114} \\ \omega_{21} & \omega_{22} & \cdots & \omega_{214} \\ \omega_{31} & \omega_{32} & \cdots & \omega_{314} \end{bmatrix} \begin{bmatrix} \overline{\alpha_1} \\ \overline{\alpha_2} \\ \vdots \\ \overline{\alpha_{14}} \end{bmatrix} \tag{18}$$

The parameters to be learned by this multilayer forward network are the connection weights ω between the fourth and fifth layers and the center value c_{ij} and width b_{ij} of the affiliation function of the second layer, respectively. The node functions for each layer are as follows:

Layer one:

$$f_1(i) = x_i a_1(i) = f_1(i) \quad i = 1, 2, \cdots, m; j = 1, 2, \cdots, n_i \tag{19}$$

Second layer:

$$f_2(ij) = -\frac{(x_j - c_{ij})}{b_{ij}^2} \quad a_2(ij) = \exp\left(f_2(ij)\right) = \mu_i^j \tag{20}$$

Third level:

$$f_3(j) = \mu_{i_1}^{i_1} \cdot \mu_{i_2}^{i_2} \cdot \cdots \cdot \mu_{i_m}^{i_m} \; Or \; f_3(k) = \min\left\{\mu_{i_1}^{i_1}, \mu_{i_2}^{i_2}, \cdots, \mu_{i_m}^{i_m}\right\} \tag{21}$$

$$a_3(j) = \alpha_j = f_3(j) \; j = 1, 2, \cdots, n; n = \prod_{i=1}^{m} n_i \tag{22}$$

Fourth level:

$$f_4(j) = \frac{a_3(j)}{\sum_{i=1}^{n} a_3(i)} = \frac{\alpha_j}{\sum_{i=1}^{n} \alpha_i} \quad a_4(j) = \overline{\alpha}_k = f_4(j) \tag{23}$$

Fifth floor:

$$f_5(i) = \sum_{j=1}^{n} \omega_{ij} \cdot a_4(j) = \sum_{j=1}^{n} \omega_{ij} \overline{\alpha_j} \quad a_5(i) = y_i = f_5(i) \tag{24}$$

If we let $y(k)$ be the desired output of the network and $y_m(k)$ be the actual output, the error is expressed as:

$$E = \frac{1}{2} e(k)^2 \tag{25}$$

$$e(k) = y(k) - y_m(k) \tag{26}$$

The learning algorithm for the network is as follows:

First define the gradient of the fifth layer as follows:

$$\delta_5(i) = \frac{\partial E}{\partial f_5(i)} = \frac{\partial E}{\partial y_i} = y(k) - y_m(k) \tag{27}$$

From there, it is sought:

$$\frac{\partial E}{\partial \omega_{ij}} = \frac{\partial E}{\partial f_5(i)} \frac{\partial f_5(i)}{\partial \omega_{ij}} = -\delta_5(i) a_4(j) = -(y(k) - y_m(k)) \overline{\alpha_i} \tag{28}$$

Then calculate the gradient of the fourth, third and second layers in turn:

$$\delta_4(j) = -\frac{\partial E}{\partial f_4(j)} = -\sum_{i=1}^{r} \frac{\partial E}{\partial a_5(i)} \frac{\partial a_5(i)}{\partial a_4(j)} = \sum_{i=1}^{r} \delta_5(i)\omega_{ij} \tag{29}$$

$$\delta_3(j) = -\frac{\partial E}{\partial a_3(j)} = -\sum_{i=1}^{r} \frac{\partial E}{\partial a_4(j)} \frac{\partial a_4(j)}{\partial a_3(j)} = \delta_4(j) \cdot \frac{\sum_{i=1, i\neq j}^{n} \alpha_i}{\left(\sum_{i=1}^{n} \alpha_i\right)^2} \tag{30}$$

$$\begin{aligned} \delta_2(ij) &= -\frac{\partial E}{\partial f_2(ij)} = -\sum_{k=1}^{n} \frac{\partial E}{\partial a_3(k)} \frac{\partial a_3(k)}{\partial a_2(ij)} \frac{\partial a_2(ij)}{\partial f_2(ij)} \\ &= \sum_{k=1}^{n} \delta_3(k) \cdot s_{ij} \cdot \exp\left(-\frac{(x_i - c_{ij})^2}{(b_{ij})^2}\right) \end{aligned} \tag{31}$$

If the minimization method is used to find f_3 and $a_2(ij) = \mu_i^j$ is the minimum input when the third layer is used:

$$s_{ij} = \frac{\partial f_3(k)}{\partial \mu_i^j} = 1 \tag{32}$$

If multiplication is used to find f_3 and $a_2(ij) = \mu_i^j$ is one of the inputs of the third layer when:

$$s_{ij} = \prod_{\substack{j=1 \\ j\neq i}} \mu_{j_i}^j \tag{33}$$

Otherwise $s_{ij} = 0$ in all other cases.
Then the first order gradient is calculated as follows:

$$\frac{\partial E}{\partial c_{ij}} = \frac{\partial E}{\partial f_2(ij)} \frac{\partial f_2(ij)}{\partial c_{ij}} = -\delta_2(ij) \frac{2(x_i - c_{ij})}{(b_{ij})^2} \tag{34}$$

$$\frac{\partial E}{\partial b_{ij}} = \frac{\partial E}{\partial f_2(ij)} \frac{\partial f_2(ij)}{\partial b_{ij}} = -\delta_2(ij) \frac{2(x_i - c_{ij})^2}{(b_{ij})^3} \tag{35}$$

Finally the learning algorithm for the parameters can be derived as:

$$\omega_{ij}(k+1) = \omega_{ij}(k) - \beta \frac{\partial E}{\partial \omega_{ij}} (i = 1, 2, \cdots, r; j = 1, 2, \cdots, n) \tag{36}$$

$$c_{ij}(k+1) = c_{ij}(k) - \beta \frac{\partial E}{\partial c_{ij}} (i = 1, 2, \cdots, m; j = 1, 2, \cdots, n_i) \tag{37}$$

$$b_{ij}(k+1) = b_{ij}(k) - \beta \frac{\partial E}{\partial b_{ij}} (i = 1, 2, \cdots, m; j = 1, 2, \cdots, n_i) \tag{38}$$

Combined with the mathematical model of the position control system of the unloading equipment, the FNN-PID control model simulation is built in Matlab, which uses S function module to encapsulate the use of the .m file written by the FNN-PID controller, which facilitates better call in Simulink.

III. C. ***Control algorithm simulation and result analysis***

Complete the design of the fuzzy neural network PID (FNN-PID) control rule base in the Fuzzy System Designer design panel and test it to get the ideal K_p, T_i, and T_d outputs and save them as a .fs file, so that they can be used to invoke the FNN-PID control algorithm later. control algorithm.

In order to achieve the optimization of container positioning and rope sway control, the “velocity-displacement dual-tracking” control strategy is used at different pixel distances with different focuses. When the robot is far away from the container, direct fuzzy velocity control is used, which has a good dynamic response of velocity tracking. When the robot is close to the container, it adopts the FNN-PID based “velocity-displacement dual tracking” strategy, which focuses on velocity tracking and displacement tracking. When the robot is close to the container, the same

FNN-PID-based “velocity-displacement dual-tracking” strategy is used, with displacement tracking as the main focus and speed gradually decreasing. When the alignment error between the spreader and the container and the swing angle of the spreader are stabilized within the allowable range, the robot brakes and the spreader starts to descend. The whole control strategy is based on the robot vision to accurately locate and track the container, and in the tracking in place at the same time to achieve the anti-rope swing control as the goal. It can be seen that in order to achieve this coordinated purpose, the speed tracking control of the robot is a key.

The comparison of the tracking effect of the ideal velocity profile and displacement profile based on fuzzy neural network PID and fuzzy PID (FPID) is shown in Figs. 6 and 7, respectively, where 6(a) and 6(b) denote the velocity tracking and response error, respectively, and 7(a) and 7(b) denote the displacement tracking and response error, respectively. It can be seen that since the output parameters K_p, T_i and T_d of the FNN-PID can adaptively change the output values based on the fuzzy rule-base with the change of inputs, the tracking effect is better than that of the FPID under the premise of reasonable rule-base design.

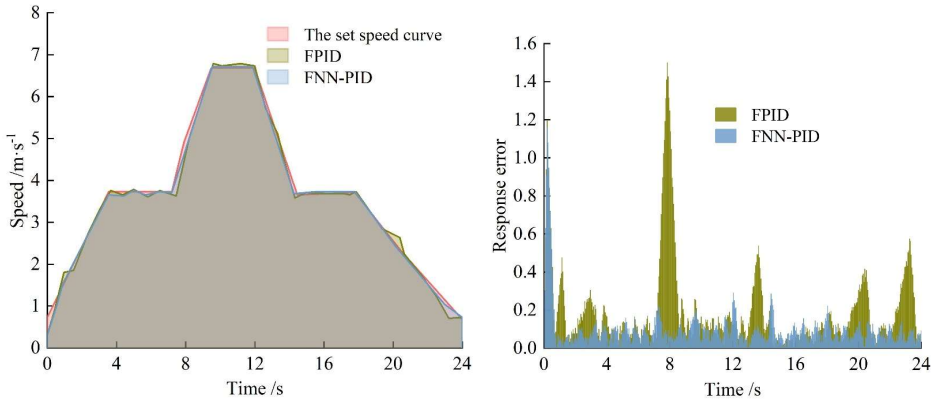

(a) Speed tracking (b) Response error

Figure 6: Speed tracking and error comparison between FNN-PID and FPID

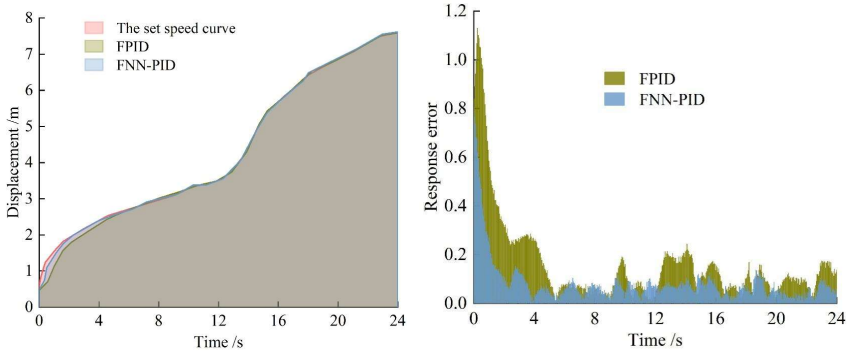

(a) Displacement tracking (b) Response error

Figure 7: Displacement tracking and error comparison between FNN-PID and FPID

In addition, the anti-sway controller of the spreader is based on the pixel distance of container positioning S and the collected swing angle of the sling θ as input variables, and then adaptively changes the three parameters of K_p, T_i, and T_d through the fuzzy neural network reasoning algorithms to follow the ideal speed curve, so that the purpose of suppressing the swing angle of the sling is achieved. The three parameters of “Setting the swing angle of the rope” are given below. The “set pendulum angle curve” is given below as the pendulum angle signal of the rope collected by the sensor, and the output pendulum angle signals obtained by tracking the speed curve with the FNN-PID and FPID control methods are shown in Fig. 8 (a) and (b), respectively.

Comparing the effect of FNN-PID and FPID anti-shaking control, it can be seen that the FNN-PID anti-shaking control can inhibit and stabilize the swing angle of the lanyard from 12 degrees to near 0 degrees within 24s, and the anti-shaking effect is obviously better than that of FPID control.

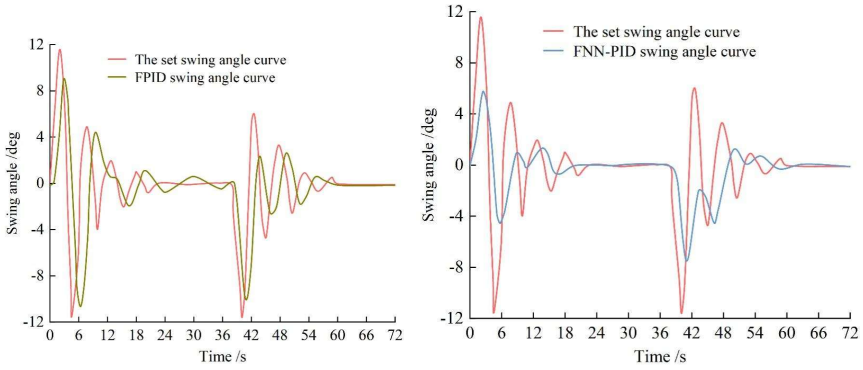

(a) Displacement tracking (b) Response error

Figure 8: Comparison of FNN-PID and FPID anti-sway control

IV. Simulation of system applications and analysis of their results

In this chapter, the application simulation in the unloading control system based on fuzzy neural network PID controller is carried out to test the system performance in three aspects, namely, guidance accuracy, visual processing effect and principle prototype unloading.

IV. A. ***Bootstrap accuracy test***

In order to verify the feasibility of robot visual guidance localization and assisted unloading in the system of this paper, the guidance accuracy test experiment is carried out in this section. The specific steps of the experiment are as follows:

(1) In a relatively flat and empty construction site, use the loading and unloading equipment to act as a target, use the handheld GPS to provide the distance between the loading and unloading equipment and the robot at a long distance, use a tape measure to measure the precise distance when the target is transverse to the distance, and the testers use walkie-talkies to communicate with each other.

(2) Turn on the system software's image field of view center scale function, the software acquisition of the image will appear in the image across the image of the horizontal and vertical lines, the intersection of which is the center of the image field of view.

(3) Place the loading and unloading equipment in front of the robot at a distance of N meters apart.

(4) The distance d between the loading and unloading equipment and the robot is obtained with a handheld GPS and the point is recorded.

(5) Capture the loading/unloading equipment target and locate it in the system software, then input the distance information and get the car's transverse deviation e by the software's calculation.

(6) Keeping the robot motionless, place the unloading equipment at the position of the longitudinal line of the image center scale so that the center of the equipment is over the longitudinal line of the image center scale and record the point.

(7) Measure the distance between two points on the ground with a tape measure.

(8) Compare the difference between the value calculated by the software and the actual measured data, i.e., the target positioning error of the system. This error is recorded as: horizontal deviation "Δe actual".

(9) According to the algorithm of mathematical modeling, when the distance error $\Delta d = 12\mathrm{m}$ or 36m, the theoretical horizontal deviation error "Δe theoretical" is calculated, respectively.

The guidance accuracy test data are shown in Table 1. It can be seen that the cross deflection error Δe obtained from the calculation of the principle prototype and the actual measurement is smaller than the theoretical error value of the mathematical modeling error analysis. When the target is at a distance of 7.2m and the ranging error is at 12m, the guided localization error of the principle prototype is 0.18m, which is within 0.2m. This proves that the principle prototype meets the system requirements in its mathematical modeling.

Table 1: Guidance accuracy test data

	d	e	Theoretical Δe ($\Delta d = 12\text{m}$)	Theoretical Δe ($\Delta d = 36\text{m}$)	Actual Δe	f
1	1800m	18.4m	0.674815m	0.887495m	0.32m	152mm
2	1800m	23.5m	0.844859m	1.135294m	0.64m	152mm
3	1600m	19.1m	0.718326m	0.958739m	0.34m	152mm
4	1300m	12.0m	0.665243m	0.848573m	0.65m	91mm
5	900m	13.8m	0.919527m	1.247185m	0.64m	50mm
6	300m	9.6m	0.954361m	1.856772m	0.63m	15.6mm
7	300m	6.2m	0.683352m	1.182643m	0.52m	15.6mm
8	150m	4.1m	0.618459m	1.257634m	0.24m	9.8mm
9	150m	12.0m	1.614351m	3.792165m	0.54m	9.8mm
10	60m	6.7m	1.423516m	3.718493m	0.71m	9.8mm
11	60m	4.2m	0.889524m	2.285164m	0.23m	9.8mm
12	7.2m	0.32m	0.205146m	Ignore this item	0.18m	9.8mm

IV. B. ***Visual Processing Quality Testing***

In this section, the visual processing quality of the principle prototype of the unloading control system is tested by taking the dock loading and unloading truck as the experimental object. The first test is the recognition test of the ground sign characters, and the test results show that the principle prototype can correctly recognize the sign characters on the ground without exception, with an average time of 0.12 seconds, and a recognition correctness rate of nearly 100%.

Then, the accuracy of the heading information of the visually calculated guide sign lines is tested. The test steps are as follows:

(1) Paste a curved marking line on the ground with 44mm wide white tape, and then paste a straight line with 38mm wide and 26mm wide white tape.

(2) When the loading and unloading truck is not started, calculate the size of the heading angle of the ground marking line and the coordinates of the center point of the marking line through the software in the principle prototype.

(3) Calculate the actual position of the center point of the marking line on the ground.

(4) Measure the center of the marking line on the ground and the size of the heading angle, and compare the results with those calculated by the principle prototype.

(5) Start the loader and repeat the above test again when the loader's engine shakes the vehicle.

The results of the marker line heading information accuracy test are shown in Table 2. It can be seen that the calculation accuracy of the principle prototype under different conditions is high, with the angular error not exceeding 0.9° and the positional error within 30 mm.

Table 2: Test data for the accuracy of heading information of the marking line

	Arc-shaped marking lines with a width of 44mm		Linear marking lines with a width of 38mm		Linear marking lines with a width of 26mm	
The vehicle engine was not launched	Angular error	Position error	Angular error	Position error	Angular error	Position error
	<0.4°	<16mm	<0.4°	<15mm	<0.4°	<15mm
The vehicle engine has been launched	Angular error	Position error	Angular error	Position error	Angular error	Position error
	<0.9°	<30mm	<0.9°	<25mm	<0.9°	<28mm

IV. C. ***Schematic Prototype Unloading Control Tests***

In this section, the system principle prototype is used for unloading control to test the jitter elimination effect during unloading. The test is conducted in 2 groups, and the test results of Group 1 and Group 2 are shown in Fig. 9 and Fig. 10, respectively, where (a) indicates without jitter compensation and (b) indicates with jitter compensation.

The test results show that during the unloading process, the marker line position error of the control system principle prototype in the image is 12-18 pixels, about 6-9 cm, after adding jitter compensation, while the heading angle error is less than 0.9° after adding jitter compensation. During the unloading experiment, the unloading control system based on robot vision can accurately reflect the heading and position changes of the unloading equipment in real time. The system navigation results in information update frequency of about 11Hz, heading information, the error is within 0.4 degrees, and the position error accuracy is of decimeter level, which is in full compliance with the requirements of the system.

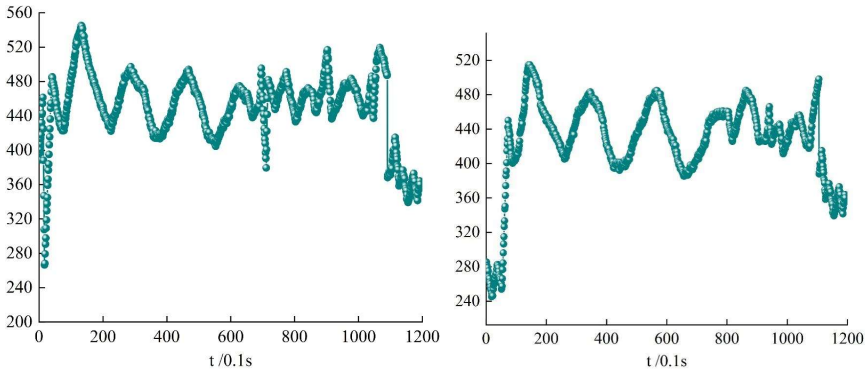

(a) No jitter compensation (b) Add jitter compensation

Figure 9: The test of Group 1

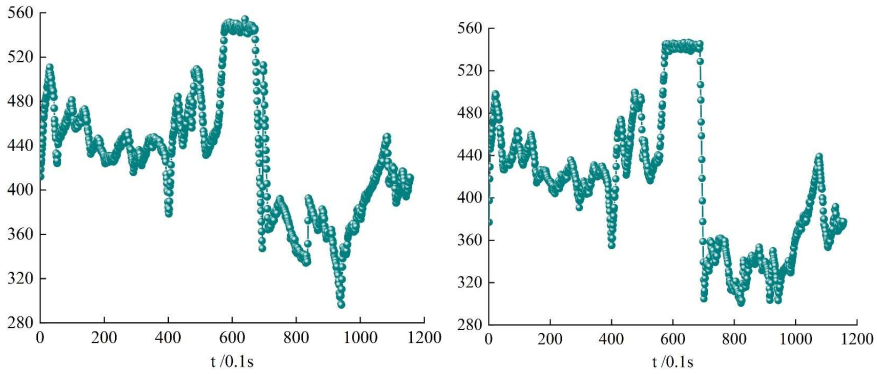

(a) No jitter compensation (b) Add jitter compensation

Figure 10: The test of Group 2

V. Conclusion

This paper builds a robot vision-guided-driven unloading control system, proposes a fuzzy neural network PID-based optimization algorithm for unloading equipment position control, and experimentally evaluates the performance of both.

The FNN-PID control algorithm proposed in this paper can adaptively change the output value based on the fuzzy rule base with the change of input, and the tracking effect is better than FPID under the premise of reasonable design of the rule base.At the same time, comparing with the fuzzy PID control algorithm, the anti-shaking effect of the FNN-PID control algorithm is better, and it can inhibit the swing angle of the lanyard from 12 degrees to stabilize it near 0 degrees in 24 s. When the target is at a distance of 7 m, the distance measurement error of the target can be reduced.

When the target is at a distance of 7.2m and the ranging error is 12m, the guided localization error of the principle prototype is 0.18m, which is within 0.2m, and the computational accuracy of the principle prototype is higher under different conditions, with the angular error not exceeding 0.9° and the positional error all within 30mm. The unloading control system based on robot vision can accurately reflect the heading and position change of the unloading equipment in real time, and the updating frequency of the navigation result information is about 11Hz, and the error of heading information is within 0.4 degrees, and the precision of positional error is at the level of decimeter, which is in full conformity with the requirements of the system.

Funding

1. This work was supported by Machine Vision Engineering Technology Center Project of Wuxi Vocational Institute of Commerce (KYPT21304).

2. Key Project of Wuxi Vocational Institute of Commerce in 2024: "Research on Teaching Methods of Electronic Technology Courses in Higher Vocational Education under Information Technology Conditions KJXJ24306".

References

[1] Hägele, M., Nilsson, K., Pires, J. N., & Bischoff, R. (2016). Industrial robotics. Springer handbook of robotics, 1385-1422.

[2] Vojić, S. (2020). Applications of collaborative industrial robots. Machines. Technologies. Materials., 14(3), 96-99.

[3] Kadir, M. A., Chowdhury, M. B., Rashid, J. A., Shakil, S. R., & Rhaman, M. K. (2015, June). An autonomous industrial robot for loading and unloading goods. In 2015 International Conference on Informatics, Electronics & Vision (ICIEV) (pp. 1-6). IEEE.

[4] Ammar, M., Ahmed, M. M., & Abdullah, M. (2022). A Chain-Driven Live Roller Mechanism for Loading and Unloading Packages on Autonomous Mobile Robots in Warehouses. Industrial Cognitive Ergonomics and Engineering Psychology, 35(35).

[5] Vicentini, F., Pedrocchi, N., Beschi, M., Giussani, M., Iannacci, N., Magnoni, P., ... & Fogliazza, G. (2020). Piros: Cooperative, safe and reconfigurable robotic companion for cnc pallets load/unload stations. Bringing innovative robotic technologies from research labs to industrial end-users: the experience of the european robotics challenges, 57-96.

[6] Auh, E., Kim, J., Joo, Y., Park, J., Lee, G., Oh, I., ... & Moon, H. (2024). Unloading sequence planning for autonomous robotic container-unloading system using A-star search algorithm. Engineering Science and Technology, an International Journal, 50, 101610.

[7] Hettiarachchi, R., Haidong, X., Zhen, L. L., Meera, C. S., & Vyas, P. (2023, October). Mobile Manipulator for Container Loading and Unloading: A Proof-of-Concept Study. In IECON 2023-49th Annual Conference of the IEEE Industrial Electronics Society (pp. 1-6). IEEE.

[8] Yuan, F., Chen, G. M., Gao, K., Zhang, J. W., & Li, Y. M. (2024, March). Design of visual assisted robot loading and unloading system. In Ninth International Symposium on Sensors, Mechatronics, and Automation System (ISSMAS 2023) (Vol. 12981, pp. 524-529). SPIE.

[9] Dmytriyev, Y., Carnevale, M., & Giberti, H. (2024). Enhancing flexibility and safety: collaborative robotics for material handling in end-of-line industrial operations. Procedia Computer Science, 232, 2588-2597.

[10] Barosz, P., Gołda, G., & Kampa, A. (2020). Efficiency analysis of manufacturing line with industrial robots and human operators. Applied Sciences, 10(8), 2862.

[11] Liu, C., Wu, J., Jiang, X., Gu, Y., Xie, L., & Huang, Z. (2024). Automatic assembly of prefabricated components based on vision-guided robot. Automation in Construction, 162, 105385.

[12] Kim, S., Lee, K. H., Kim, C., & Yoon, J. (2024). Vision-centric 3D point cloud technique and custom gripper process for parcel depalletisation. Journal of Intelligent Manufacturing, 1-17.

[13] Giannoccaro, N. I., Rausa, G., Rizzi, R., Visconti, P., & De Fazio, R. (2024). An Innovative Vision-Guided Feeding System for Robotic Picking of Different-Shaped Industrial Components Randomly Arranged. Technologies, 12, 1-26.

[14] Liang, J., Ye, Y., Wu, D., Chen, S., & Song, Z. (2024). High-efficiency automated triaxial robot grasping system for motor rotors using 3D structured light sensor. Machine Vision and Applications, 35(6), 132.

[15] Chen, Z., Li, T., Qin, L., & Jiang, Y. (2025). Vision-Guided Autonomous Block Loading in a Dual-Robot Collaborative Handling Framework. Journal of Construction Engineering and Management, 151(5), 04025035.

[16] Kang, J. S., Kang, J. K., Son, S., Park, S. H., Jung, E. J., & Cho, G. R. (2024). Image Enhancement Method for Detection in Logistics Loading and Unloading Robots. IEEE Access.

[17] Ashish Sharma, Manoj Kumar Kar & Harsh Goud. (2025). A novel modified grey wolf optimization tuned PID controller with fractional filter for the CSTR system. Heat and Mass Transfer,61(4),36-36.

[18] Siyu Gui, Guodong Zhang & Qiang Xiao. (2025). Projective synchronization in fixed/preassigned time of discontinuous fuzzy neural networks with mixed-time delays. International Journal of Dynamics and Control,13(4),136-136.

[19] Hongyang Wei, Ning Zhu, Zhenyang Sun, Sichao Tan & Ruifeng Tian. (2025). Research on the intelligent control strategy of pressurizer pressure in PWRs based on a fuzzy neural network PID controller. Nuclear Engineering and Design,433,113875-113875.